# 2. ACCELERATOR AUGMENTATION PROGRAM

## 2.1 HIGH CURRENT INJECTOR

The High Current Injector (HCI) Project will accelerate the ion beam from ECR source using normal temperature Radio-Frequency Quadrupole (RFQ), IH type Drift Tube Linac (DTL) and superconducting low beta cavity module to match the input velocity at our existing superconducting linear accelerator.

### 2.1.1 HIGH TEMPERATURE SUPERCONDUCTING ECRIS-PKDELIS AND LOW ENERGY BEAM TRANSPORT (LEBT)

G. Rodrigues, Y. Mathur, P. Barua, A. Kothari, Chandra Pal, R.Ahuja, A.J.Malyadri, U. K. Rao, A.Mandal & D.Kanjilal

**a) Replacement of faulty high current feedthroughs in both cryo-coolers**

The high current feedthroughs ('styecast' based) in both cryostats were found to be leaking simultaneously and was most probably attributed to an aging effect of the styecast glue over an approximate period of 12 years of continuous operation. Since these feedthroughs had been custom made for the cryostats in the original design, it was decided that similar high current feedthroughs could be ordered from Scientific Magnetics, U.K in order to get the system back in working condition. All the feedthroughs were carefully de-soldered with utmost care to avoid damage to the signal cables as shown in figure 2.1.1 below. Multi layer insulation (MLI) layers were freshly installed with a total of ~ 25 layers after replacing the new feedthroughs. After a thorough vacuum pumping for couple of days, system was powered up and the ion source resumed normal operation. After a year of operation, it was observed that both the feedthroughs on the extraction cryo-cooler were found to be leaking. However, those on the injection side were found to be OK. It was decided to replace the two feedthroughs at the extraction side with 'ceramic to metal' bonded feedthroughs (Figure 2.1.2). In the near future, it is planned to replace the feedthroughs on the injection side with 'ceramic to metal' bonded feedthroughs.

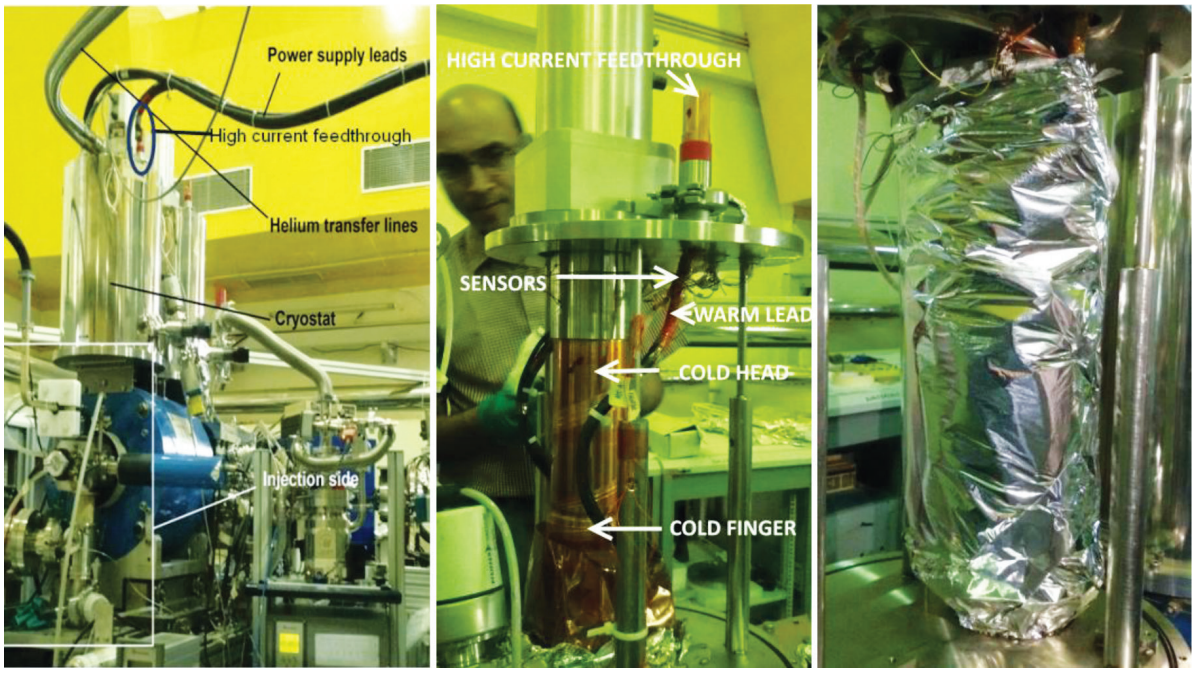


Figure 2.1.1 (Left) View of the 18 GHz HTS ECR Ion Source
(Middle) Inside view of one of the cryostats
(Right)View of the MLI wrapping around the cold head

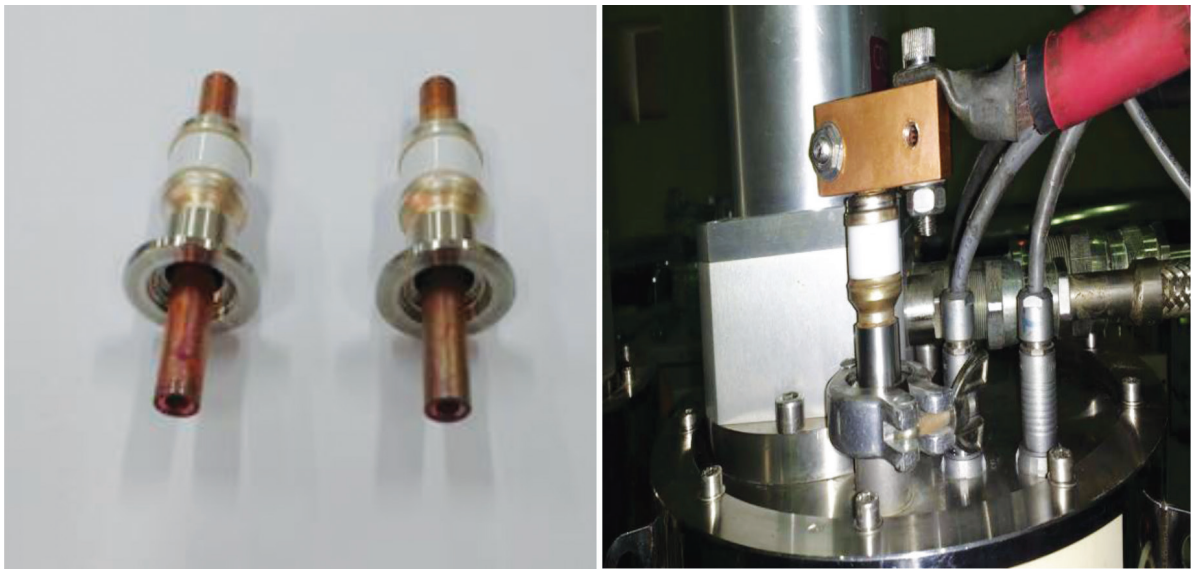

Figure 2.1.2 (Left) View of the 'ceramic to metal' bonded feedthroughs (Right) View of the assembly on the extraction side

### b) Optics through the modified LEBT

As reported in the previous year annual report, the LEBT was modified to correct for double focusing after the analysing magnet using a steerer placed just after it. Additionally, the electrostatic quadrupole doublet was replaced by a magnetic quadrupole singlet. The beam transmission at the position of the diagnostic box after the analysing magnet was measured to be ~ 80 %, nearly 100 % at the following downstream Faraday cup (just outside the high voltage platform), while the beam transmission at the first Faraday cup (before analysis) was only a small fraction of the drain current. Injection vacuum was further improved by installing an additional turbo pump. The extraction optics in the new, movable extraction system is shown in figure 2.1.3 and optics through the LEBT on the 200 kV high voltage platform in the old and modified configuration is shown in figure 2.1.4.

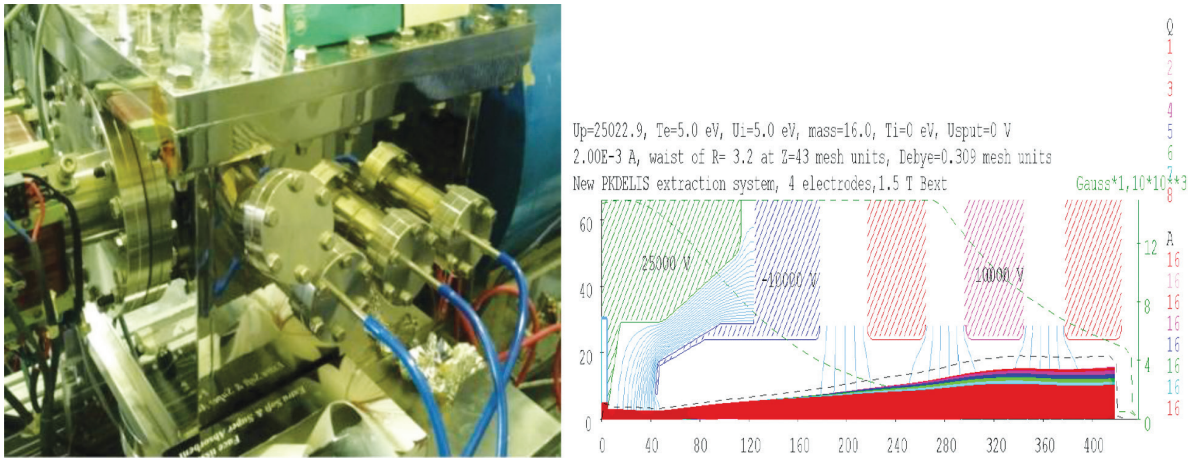


Figure 2.1.3 (Left) View of the movable extraction system ; (Right)Extraction optics of the movable extraction system

Contradictory to the ion optics simulations, it has been observed that beam intensity losses occur between the ion source and the analysing magnet due to the large distance between them mainly due to the incorporation of diagnostic elements. Efforts are underway to minimise the distance as much as possible by avoiding the diagnostics and to couple the ion source as close as possible to the analysing magnet. The effects of misalignments of the movable extraction system show that the magnetic steerer values (positioned after the movable extraction system) in X and Y were not comparable. It has been observed that vertical steering effects are more dominant than in the horizontal plane.

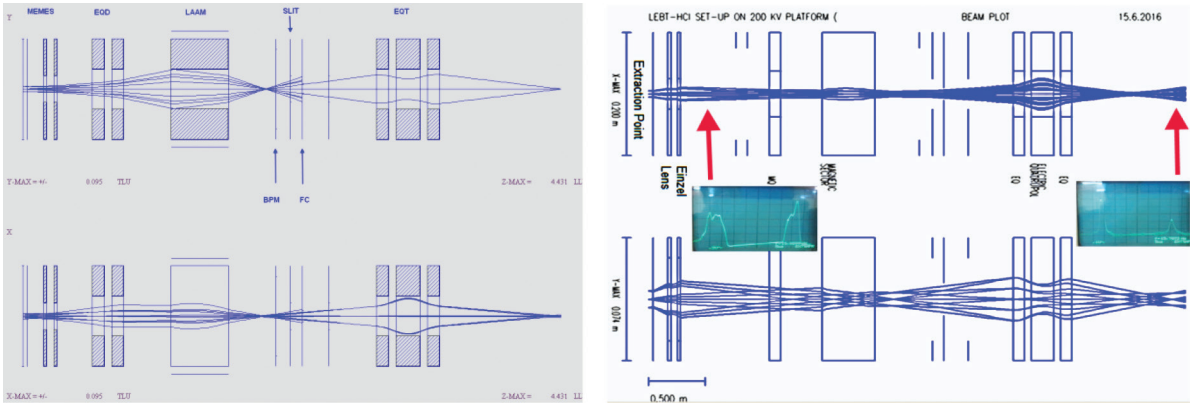


Figure 2.1.4. (Left: old configuration) (Right: modified configuration) Optics through the LEBT on the 200 kV high voltage platform

## c) Installation of water-cooled cryo-coolers with a dedicated water chiller

Our experience has shown that over a period of 10 to 12 years, air-cooled cryo-coolers have demanded a lot of maintenance due to dust and high temperature environments. This eventually makes the ion source running period limited. The history of operation of the cryo-coolers was recently reported in the international conference, ICEC 26- ICMC 2016 (Figure 2.1.5) [1]. In order to resolve these issues, it was decided to use water cooled cryo-coolers to ease the maintenance of the cryo-coolers. This would eventually facilitate a smoother operation considering the wide range of temperatures encountered while running the various systems on the high voltage platform. A view of the installed water cooled cryo-coolers together with a water chiller is shown in figure 2.1.6. After they were installed and commissioned, the performance has been very satisfactory with minimum maintenance requirements.

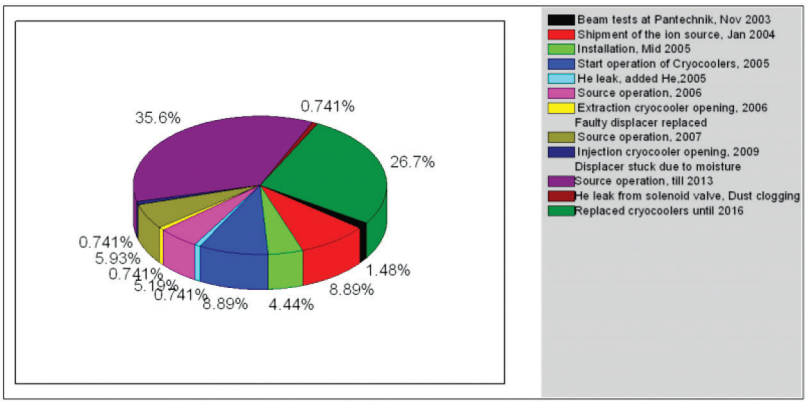


Figure 2.1.5. Brief history of operation of cryo-coolers from the year 2003


Figure 2.1.6. View of the newly installed water cooled cryo-coolers together with a dedicated water chiller

## d) Acceleration using platform voltage and initial beam bunching measurements

In order to begin the process of bunching before injection into the radio frequency accelerator (RFQ), the dc beam from the HTS-ECR ion source was further accelerated using the platform voltage and initial bunching measurements were performed with the downstream multi-harmonic buncher. Using a beam of $N^{3+}$, a bunched

beam of 5 ns was obtained and detected using a fast Faraday cup placed downstream of the buncher, just before the entrance of the RFQ. It is expected that the bunch width can be further improved by closing the post-analyser slits to define the beam trajectory and further improving the beam tuning from the ion source. Initial measurements are being carried out to see the effects of the beam trajectory path. Later, the effects of the energy spread from the ion source will be tried to be minimised to improve the bunched beam width.

### e) Electronics work and developments

1) New water cooled cryo-coolers were installed and interlocked with the chillier and power supplies electronics.

2) High voltage deck power supply installed along with the 5V enable signal and door interlocks.

3) Multi Harmonics Buncher (MHB) tank electronics has been tuned to the required frequencies on the dummy load.

4) RF interlock for klystron power generator was not coming properly due to plasma chamber cooling unit even though the cooling was fine. It was diagnosed; the problem was due to improper functioning of water flow sensor of the cooling unit. It had been repaired and minimum required flow setting had been done. It is now providing the correct interlock signal for the microwave generator.

Figure 2.1.7. (Left) PKDELIS ECR Ion source on high voltage platform and (Right) HV platform power supply

5) 6V, 200A solenoid power supply for the extraction coil was not coming to the ready state even though all the required interlocks were ok. On detail checking of this Xantrex power supply, we diagnosed that one opto-coupler at its shutdown signal circuit was faulty. We replaced the IC and solved the problem.

   Then after some time we faced problem of frequent tripping of solenoid coil power supplies. On detailed checking we diagnosed that it was due the noise pickup by the coil power supplies cables form the cryostat chillier unit. We re-routed the cables and moved the solenoid coil control electronic rack slightly away from the chillier unit and thus solved the problem.

6) We faced problem with klystron power generator, it was not coming to ready state in a stable manner. Its ready state come and goes very frequently. We found that this problem was due to faulty vacuum gauge controller which was providing the interlock signal for microwave. We replaced the vacuum controller and solved the problem.

7) The needle gas valve controller had gone bad due to which we were not able to control the gas flow for the plasma generation. On detailed checking we diagnosed that it was due to the fault in the negative power supply filter section of this controller. We replaced the filter capacitors of the negative power supply and thus solved the problem.

8) 50kV high voltage power supply for the source extraction was not working properly. It was not going beyond 2kV. On detailed checking and analysis we found that it was due to the high voltage output cable whose insulation has gone bad. We replace the cable and solved the problem. It is now working properly.

9) Klystron based 2kW, 18GHz microwave power generator for PKDELIS ECR ion source had gone bad. It was not properly coming to ready state. Its high voltage for activating and powering the klystron was not getting ON even after ready ok signal. On checking we found that it was due to fault in its CD control unit. On detailed checking and analysis of this control unit circuitry we found that it was due to two relays which were not working, including some diodes. We replaced the faulty components and solved the problem. This microwave generator is now working properly and is being used regularly.

10) Plasma Chamber chiller main ON/OFF switch, which is of special type, had gone bad due to which we were not able to operate it properly. We replaced the switch and solved the problem.

11) We faced problem with the pre- amplifier for fast Faraday cup signal. It had gone bad and we were not able to tune the beam properly through MHB. We faced problem while repairing this preamplifier since its circuit diagram was not available for servicing it. So we had to first trace its circuit and then had decoded the smd codes of faulty components. We then repaired it successfully by replacing the faulty components.

12) Routine maintenance of high voltage and RF related system were carried out, which includes cleaning of high voltage bleeders, microwave generators internal high voltage section cleaning, cleaning of DC break and second deck.

**REFERENCE**

[1] G.Rodrigues, Y.Mathur, U.K.Rao, P.S.Lakshmy, A.Mandal, A.Roy and D.Kanjilal, IOP Conf. Series: Materials Science and Engineering 171 (2017) 012069

## 2.1.2 STATUS OF THE MULTI-HARMONIC BUNCHER FOR THE HIGH CURRENT INJECTOR

A Sarkar, Sarvesh Kumar, Rajesh Kumar, R Ahuja, S K Suman, Y Mathur, P Barua, A Kothari, A J Malyadri, V V V Satyanarayana, B P Ajithkumar

The MHB vacuum chamber which was installed in the HCI beam line after the high voltage deck was properly aligned with the different components of the beamline. Then the molybdenum grids placed in the grid assembly were installed inside the chamber with proper supporting rods connected to the specially designed ceramic RF feedthroughs. These grids formed the single gap across which the beam bunching is done. An ion pump was installed near the chamber to maintain a vacuum of the order of $10^{-9}$ torr inside the MHB chamber.

The tank circuit assembly housed on the copper base plate was mounted on top of the vacuum chamber and necessary RF connections were made. A closed loop de-ionised water cooling system comprising of two pumps and a temperature controlled chiller was installed permanently near the MHB chamber and proper inlet and outlet connections were made to cool the tank circuit coils. The closed loop cooling system was tested thoroughly with satisfactory results A final tuning of the tank circuit elements with proper coupling was done. We could achieve all the desired frequencies after several iterative tuning procedures. Doubly shielded RF cables were laid from the MHB chamber area to the local control console and permanent patch panel connections were made.

The total control electronics for MHB was installed in the local control console and the RF power amplifier and other accessories were assembled on the rack just below the MHB chamber. The controller and other accessories were integrated to the system. The controller was tested along with the system for several days. All the phase and amplitude lock loops performed satisfactorily. The saw-tooth voltage was generated and its long term stability test was performed.


Figure 2.1.8 Tuned frequencies as seen on VNA

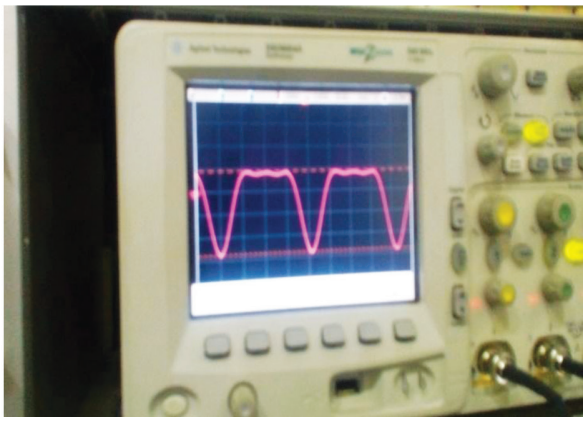

Figure 2.1.9 Differentiated saw-tooth signal as seen on CRO

This was followed by a beam test. $^{14}N$ beam with +4 charge state generated by the ECR source was successfully bunched by the MHB. A fast faraday cup installed just before the entrance of the RFQ was used to detect the beam bunching. Beam bunches of 4ns FWHM was seen directly on the oscilloscope. The power required for optimum bunching was approximately 15 Watts. With proper source tuning and reducing the energy spread

introduced by the source and the bending magnet better FWHM can be achieved in future. Spare grids have also been successfully brazed on copper cones by vacuum furnace technique.

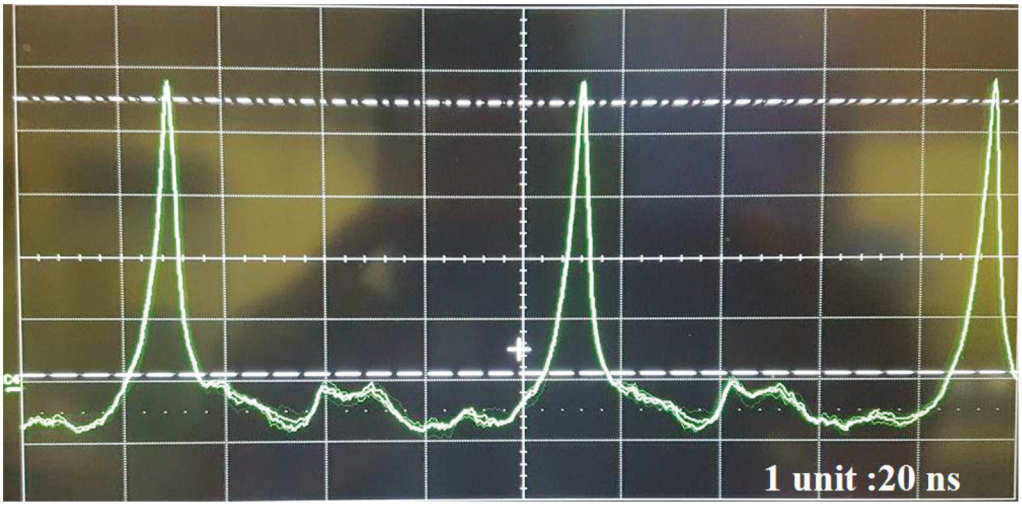


Figure 2.1.10 Beam bunches with 4ns FWHM as seen on CRO

### 2.1.3 HIGH POWER RF TESTS ON RADIO FREQUENCY QUADRUPOLE

Sugam Kumar, R. Ahuja, A. Kothari, C.P. Safvan

High power tests have been done to check the frequency and temperature stability and also to survey both the rf and X-rays leak from the 4-rod RFQ operating in cw mode at 48.5MHz to accelerate the ion beam of A/q ≤ 6 produced by the ECR from 8keV/A to 180keV/A. Resonant frequency variation as a result of non-uniform temperature distribution from RF heating in the RFQ is difficult to simulate and predict. The sensitivity of resonant frequency to RF power has been measured as part of the RF power testing. It is observed that maximum shift in frequency appears in low power range, as it is shown in fig. 2.1.11a, that up to 8kW shift is 87kHz while from 8kW to 32kW shift is only 11kHz.

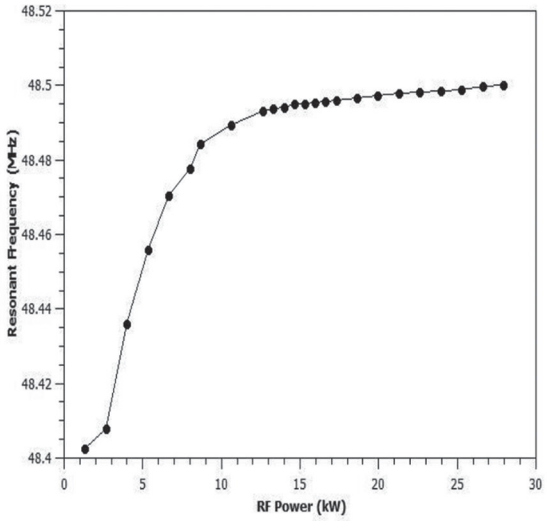


Fig. 2.1.11 (a)

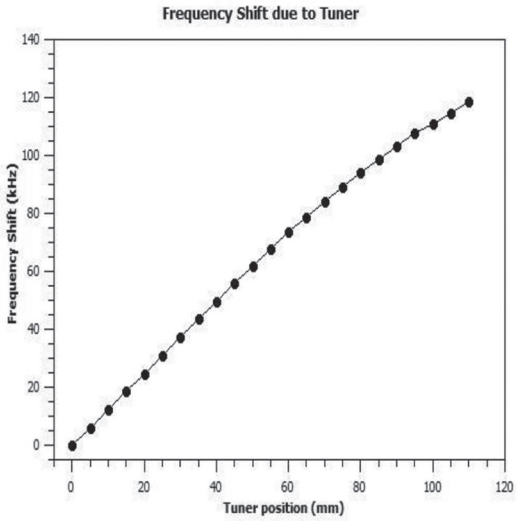


Fig. 2.1.11 (b)

In order to keep the resonant frequency of cavity at designed value of 48.5MHz, a inductive tuner is designed. The tuner plunger is made of copper and water cooled which can move inside the cavity by 110mm and produces the frequency shift of 120 kHz as shown in fig. 2.11.11b. In order to match the frequency of the cavity, a frequency control loop system is designed to move the tuner in and out during operation.

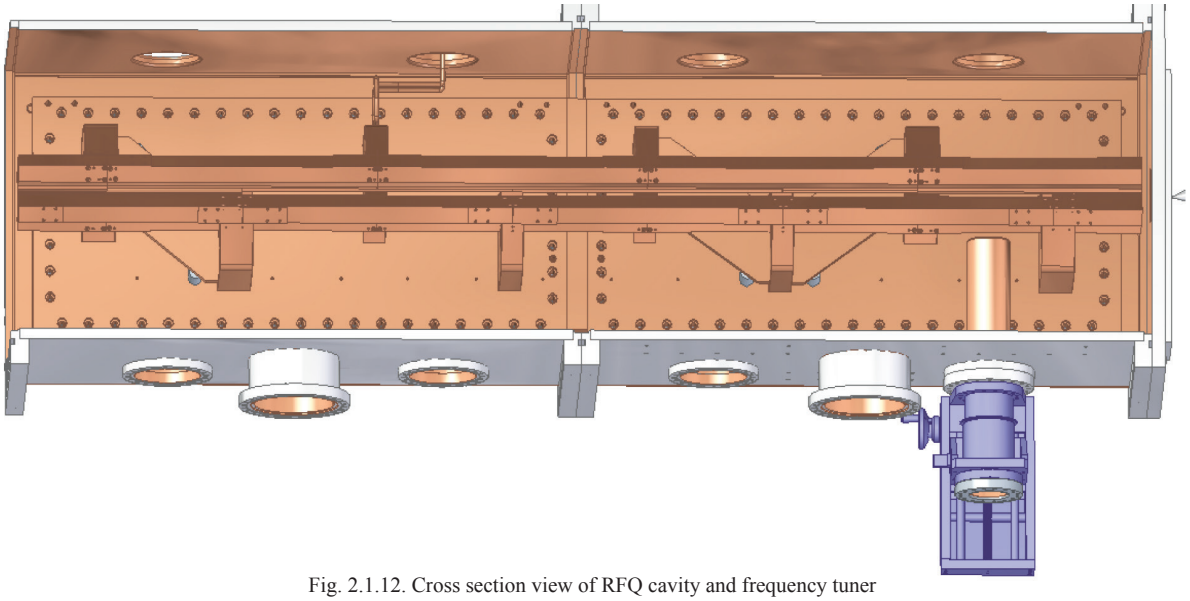

Fig. 2.1.12. Cross section view of RFQ cavity and frequency tuner

Two turbo pumps have been used to create base pressure of 3x10-8 Torr. This much pressure before application of RF power, is acceptable for beginning power tests. Fast interlocks for reflected power, water and vacuum to the RFQ were also installed. During test, power was fed in small steps as there was huge degassing with rise in temperature of cavity.

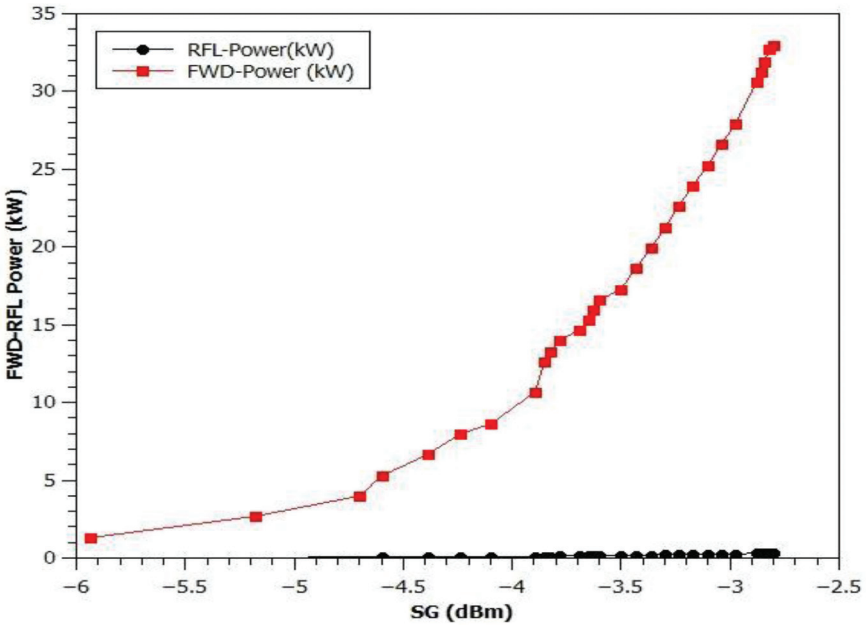


Fig. 2.1.13

During the high power test we also found that coupling coefficient decreases gradually with increasing forward power. We resolved this problem by operating RFQ in over-couple condition. A commercial 120kW rf amplifier is being used to deliver power in the cavity. In the first test, 32kW power has been fed in the cavity with minimum reflection of 320W. We observed Marginal rise in water temperature from 19ºC to 21ºC at 32kW. Very small but non-uniform local heating also observed at the bottom SS chamber. Base pressure increased from 4 x $10^{-9}$mbar with no rf power to 1.3 x $10^{-8}$ mbar at 32kW. Electromagnetic radiation was undetectable in the lowest range of commercial survey meter at this power. X-rays leak was examined with the survey meter at several points on the outer surface of cavity, the X-ray leak was less than 15 µR/h. We are preparing RFQ cavity for rf conditioning up to 80kW which is the expected power level to generate required 70kV inter-electrode voltage in order to accelerate ions from 8 to 180keV/A.

### 2.1.4 Drift Tube LINAC Resonator

Ajith Kumar B P, J. Sacharias, R Mehta, V V V Satyanarayana, R V Hariwal, S Kedia, Rajesh Kumar, S. Venkataramanan, B K Sahu and P Barua

The DTL resonator #1 had been tested for continuous operation at 5kW power. The amplitude and phase control circuits were tested up to 2 kW, beyond which the temperature control need to be incorporated in order to the control loop.

The work on the second resonator is progressing. The tank body and accelerating tube support structures of the remaining four resonators have been completed. The drift tube fabrication and assembly is remaining. The support structure for the DTL has been designed and fabrication started.

RF Power amplifiers for the first three resonators have been procured. The 20 kW solid state power amplifier has been tested for continuous operation. The 28 kW power amplifiers for the remaining resonators is under processing.

Layout of the beam line components is almost final. The fabrication drawing for DTL support structure also is getting completed. The detailed planning of electrical power and cooling water requirements has been completed and tenders will be floated.

### 2.1.5 Travelling Wave Chopper

S Kedia, Rajesh Kumar and R Mehta

The Low Energy Beam Transport (LEBT) section of the High Current Injector (HCI) incorporates a Travelling Wave Chopper (TWC). The compact TWC has been designed to remove dark current and produce the short bursts of ions at different repetition rates. The TWC has been designed to select 60 ns of beam at the different frequencies of 4, 2, 1, 0.5, 0.25 and 0.125 MHz. The distinguishing feature of the design is use of a multi-plate deflecting structure with reducing capacitance to optimize the electric field which results in higher efficiency in terms of achievable ion current. To maximize the effective electric field and its uniformity, gap between the deflecting plates has been varied from 15 mm to 24 mm and a semi-circular contour has been incorporated (Fig.-2.1.14). The electric field variation seen by the charged particles along the beam direction is less than ±0.5% within the plate length. The length of deflecting plates was chosen to reduce the beam loss. Since the velocity of the charged particles in the LEBT section is constant, therefore the separation between two successive set of deflecting plates has been kept constant to match the ions transient time which is 32 ns. Instead of sinusoidal, a square pulse was chosen to increase the transmission efficiency and to decrease the tailing effect. The loaded capacitance of structure was kept <10 pF to achieve fast rise/fall time of the applied voltage signal. A python code has been developed to verify the various design parameters. The simulation also shows that one can obtain efficient deflection of unwanted particles, with >90% transmission efficiency for the desired particles. In order to examine the validity and feasibility of physical design, various simulations, namely Solid Works, TRACE 3D, CST MWS and homebrew python codes were carried out.

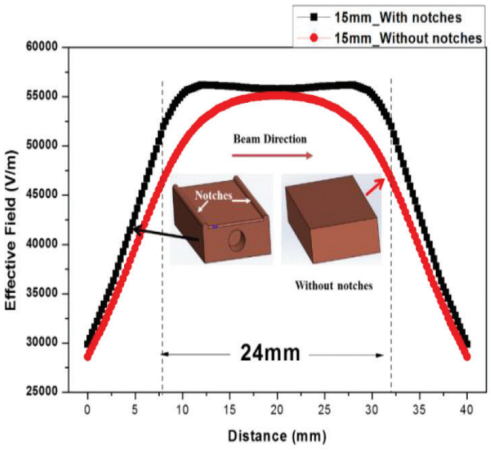


Fig.2.1.14. The improvement in the net electric field and linearity in the transient region due to the introduction of the semi-circular contours.

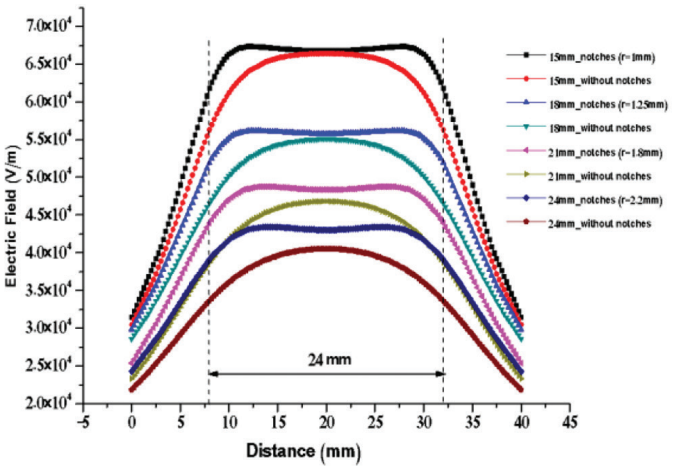


Fig.2.1.15. The improvement in the net electric field and linearity in the transient region due to the formation of semi-circular contours.

#### Plate Design Modifications:

To further increase the efficiency of TWC, semi-circular contours were incorporated in the design (Fig.2.1.14) to achieve maximum electric field within the deflecting plates and to reduce the emittance growth of the beam. The contours of the different radius were incorporated at the entrance and exit sides of the deflecting plates. The radius of contour was optimized to achieve constant field throughout the plate length. By varying the radius of contours, linearity, within ±0.5%, in the transient region has been increased by a factor of two as compared to the original design (Table 1). The total voltage seen by the particles in the transient region has been further increased by 3.8%, 5%, 7.6% and 10.8% for set1, set2, set3, set4 respectively (Table 1). The radial component

of the non-uniform electric field gives rise to the emittance growth and the emittance growth is proportional to the radial component of the electric field seen by the particles. Therefore, with the inclusion of the contours, the emittance growth has been minimized.

The Fig. 2.1.15 represents the first set of a plate having 15 mm gap between deflecting plates. The radius of a contour is 1.0 mm. The field seen by the charged particles along the beam direction is 3.8% more compared to original design and linearity within ±0.5% is almost double compared to an original design. The voltage variation seen by the charged particles became almost half (Table 1).

.

**Table-1. The percentage increase in the effective voltage and linearity due to contours.**

| Length along the beam line | Shape of deflecting plates | Total Voltage (V) ($E_z dZ$) Area Under the curve | % Increases in Area | Linearity (± 0.5 %) | Voltage Variations along the plate length (24mm) |
|---|---|---|---|---|---|
| Set-1 15mm | Modified (r=1mm) | 1598708 | 3.8% | 19mm | 8% |
| | Unmodified (r=0mm) | 1539835 | | 10mm | 15.2% |
| Set-2 18mm | Modified (r=1.25mm) | 1334228 | 5% | 19mm | 7.5% |
| | Unmodified (r=0mm) | 1269894 | | 8.5mm | 15.3% |
| Set-3 21mm | Modified (r=1.8mm) | 1151771 | 7.6% | 17mm | 9.8% |
| | Unmodified (r=0mm) | 1069462 | | 7mm | 17.2% |
| Set-4 24mm | Modified (r=2.2mm) | 1024028 | 10.8% | 16.5mm | 9.9% |
| | Unmodified (r=0mm) | 923591 | | 7mm | 17.0% |

The data analysis was carried out for all the set of deflecting plates and results are tabulated in Table 1 above. The field seen by the charged particles have been increased by 3.8%, 5%, 7.6% and 10.8% for the set1, set2, set3, set4 respectively. The linearity along the path of charged particles became almost, double in all cases. The voltage variation seen by the charged particles has been reduced by a factor of half. Consequently, emittance growth for the desired charged particles has been reduced.

### Mechanical Structure

The eight deflecting plates of OFHC copper and all other mechanical components like ceramic bushes, spacers, top/bottom plates etc. were fabricated and assembled with the accuracy of ±100µm. The semi-circular contours of the different radius were incorporated. The inner mechanical assembly shown Fig.3 has been fabricated and assembled. The outer housing of travelling wave chopper has been designed and order has been placed for fabrication. The outer chamber is having its inbuilt flanges on the both sides to install in the beam line. The Fig. 2.1.16a and 2.1.16b present its isometric and front view respectively.

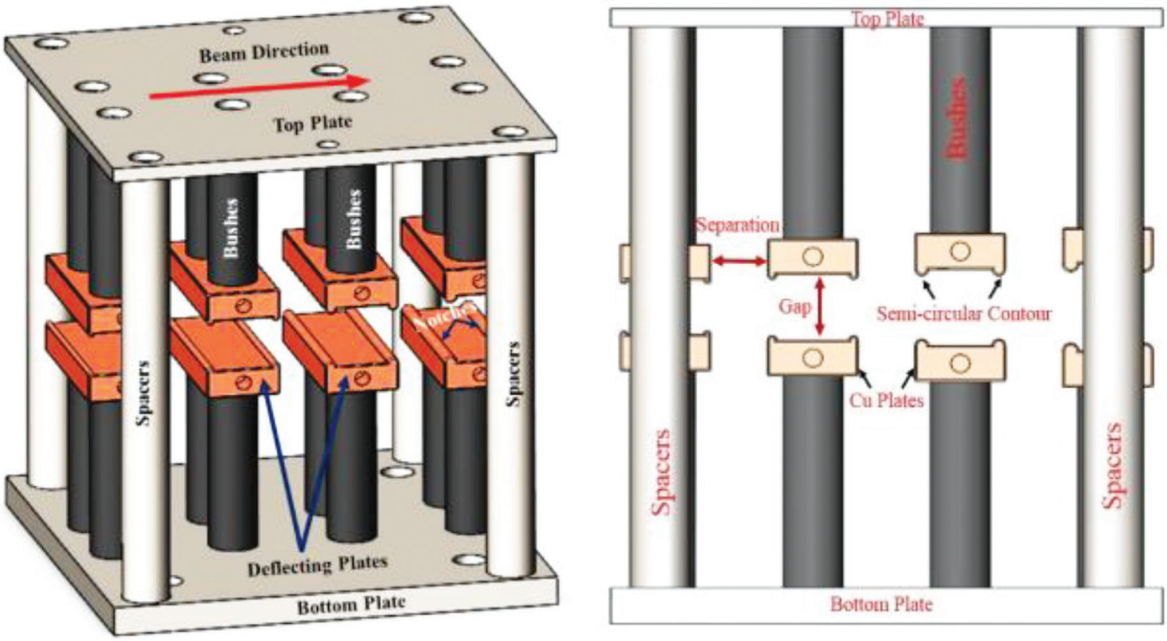


Figure 2.1.16 The inner mechanical assembly of TWC, (a) trimetric view, (b) side view

### 2.1.6 48.5 MHz Spiral Buncher for MEBT Section of HCI

R Mehta, R Ahuja, S Kedia

A 48.5 MHz spiral buncher has been designed and developed to match the longitudinal emittance between RFQ and DTL. The RF characterization was carried out to measure the resonant frequency and quality factor, bead pull technique was used to measure the electric field profile along & off the beam axis. The measured resonant frequency was 48.615 MHz as compared to the design value of 48.5 MHz. The measured quality factor was ~2800 (design value based on the CST MWS is 3900). To improve the quality factor buffing of spiral and inner copper surface was done. After buffing the quality factor was 3800. The spiral buncher cavity was assembled and leak tested up to $1x10^{-8}$ mbar. A vacuum leak was detected through the cooling channel of the spiral section. The high-power coupler was installed and loop was optimized for 50 ohm (Figure 2.1.17).


Figure 2.1.17 Cavity after buffing, the power coupler and 50 ohm matched condition of the loop

**Bead Pull Measurement:**

The beadpull setup was installed (Figure 2.1.18) and measurement was carried out to validate the electric field profile and to measure the stored energy. The off-axis measurement was also carried out to find out the uniformity of the field between gaps. The bead pull results are summarized below. A Teflon bead of 2mm diameter was used. Initial measurement shows that second gap is shorter as compared to the first gap (Figure 2.1.19a). From the data of frequency shift it can be calculated that the second gap is ~ 2.2 mm shorter. During the alignment it was possible to fix only one gap very accurately due to the mechanical constraints. The first gap was fixed to 20.5

mm (the design value) within ± 50 microns. After correcting the second gap length uniform field distribution was observed (Figure 2.1.19b). The stored energy was calculated to be ~12 mJ using the bead pull data. The measured electric field profile and stored energy matches very well with the theoretical model using CST MWS.

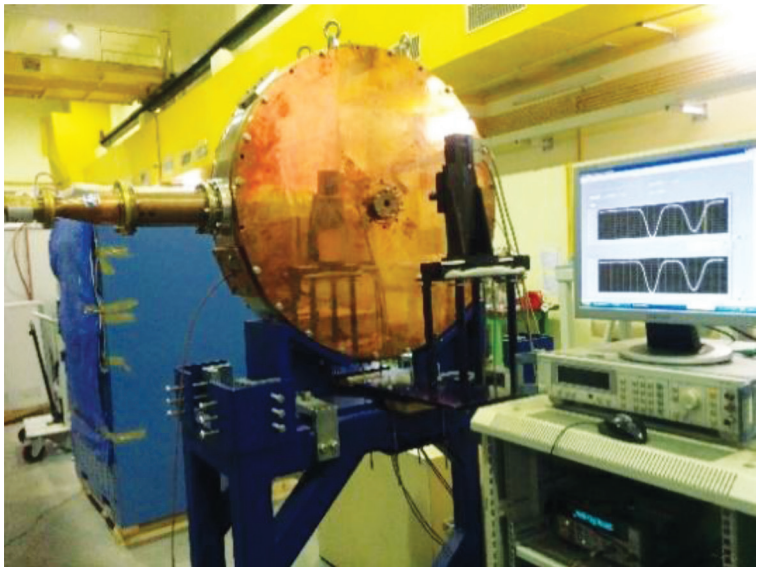

Figure 2.1.18 Bead Pull setup

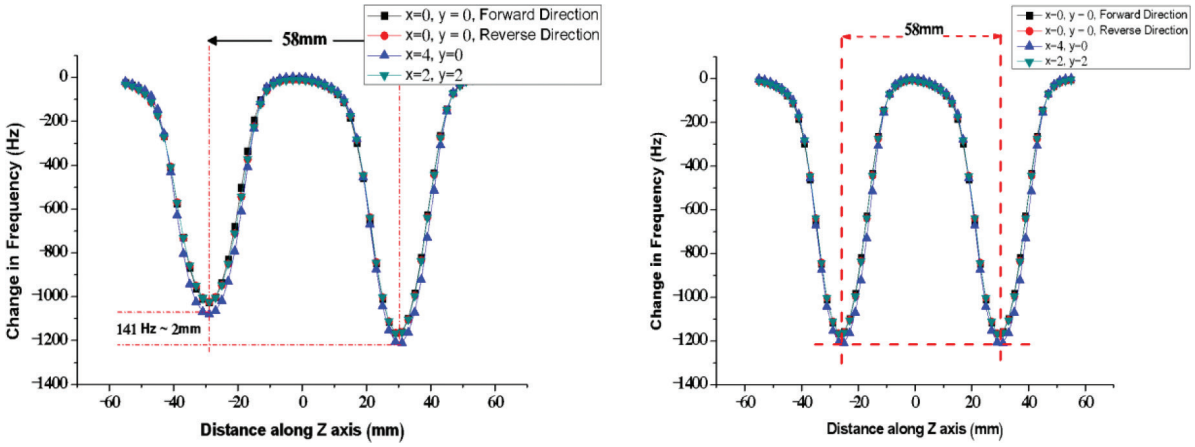


Figure 2.1.19: a) Initial Electric Field Profile and b) Electric Field Profile after Gap Correction

### 2.1.7 Beam Transport System for HCI

Sarvesh Kumar, G. Rodrigues

This year, beam optics of HCI has been revised again in order to commission the beam in real time for low energy beam transport section of HCI. The dc beam has been successfully tuned first to the entrance of RFQ. Then it is tuned in the bunched form using the multiharmonic buncher (MHB) and we are able to obtain 4 ns as bunch width. The beam transmission is 60% through buncher and after buncher, it is 100% till the entrance of RFQ. In future, the transmission through buncher has to be improved as well as the beam has to be bunched to better than 2 ns.

#### 2.1.7.1 Beam optics of LEBT and MEBT section of HCI

Sarvesh Kumar, G. Rodrigues

The LEBT section is designed to be as compact as possible to minimize the blow up of low energy beams. The beam is extracted at 20 kV using a multi-electrode movable extraction system and is focused parallel in the gap of large acceptance analyzing dipole magnet. The beam is then further transported and accelerated using a combination of an electrostatic quadrupole triplet and an accelerating column respectively to an image point located at the position of the multi-harmonic buncher (MHB). The dc beam is bunched by MHB close to the

entrance of RFQ. After the MHB, the beam is matched transversely to the design parameters of RFQ with a set of four magnetic quadrupoles (Q1,Q2,Q3,Q4). Two magnetic steerers, one before Q1 and other in between quadrupoles Q2 and Q3, are placed to correct beam position inside RFQ. Before RFQ, beam optics for four quadrupoles is studied for following two different modes and is shown in Fig. 2.1.20.

Case-1: Point to Point (FDDF in X-plane, DFFD in Y-plane)
Case-2: Point to Parallel to Point (FDDF in X-plane, DFFD in Y-plane)

Here F stands for focusing and D stands for defocusing. Both configurations would be tried to optimize the transmission as well as beam quality close to the entrance of the RFQ. For case-1, Twiss parameters matches very well with the design values for RFQ but for case-2, they differ slightly in transverse plane. The magnetic quartet structure performs in the same field configuration of a magnetic quadrupole triplet but it gives flexibility in both cases to put a magnetic steerer at the middle to steer the beam inside RFQ for optimization of its transmission. MHB require less than 1kV with add-on harmonics to match the beam in longitudinal phase space. All the quadrupoles of LEBT section are developed indigenously developed in IUAC. With the new configuration, the beam optics of LEBT, RFQ and MEBT was rechecked using TRACK code as shown as in Fig. 2.1.22.

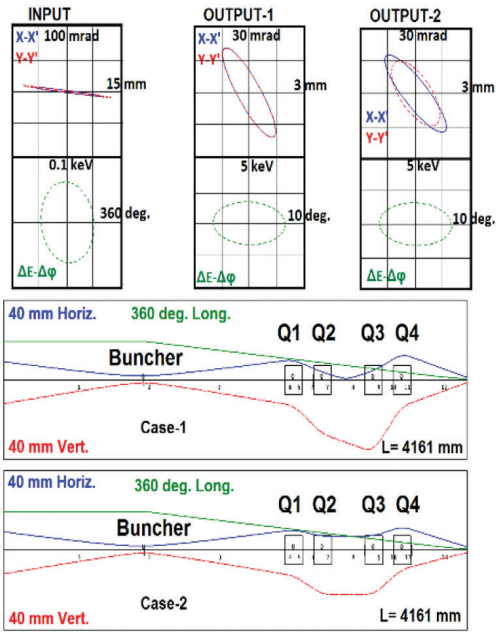


Fig 2.1.20. Beam optics in the LEBT section

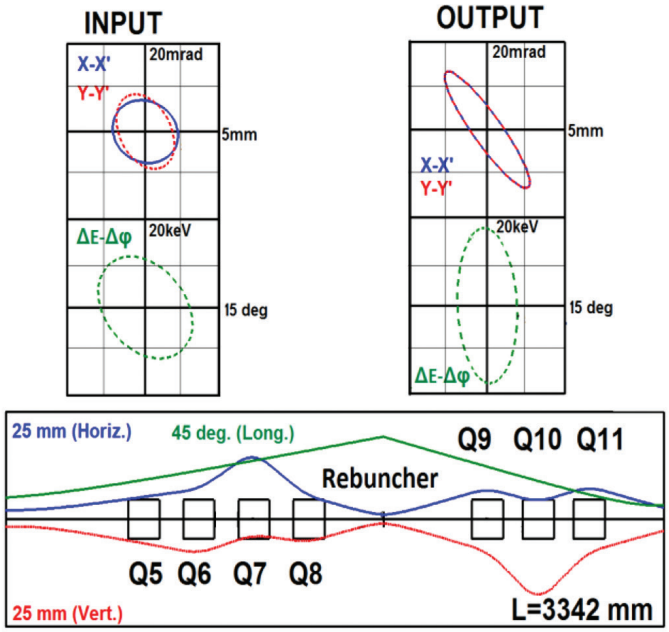


Fig 2.1.21 Beam optics in the MEBT section

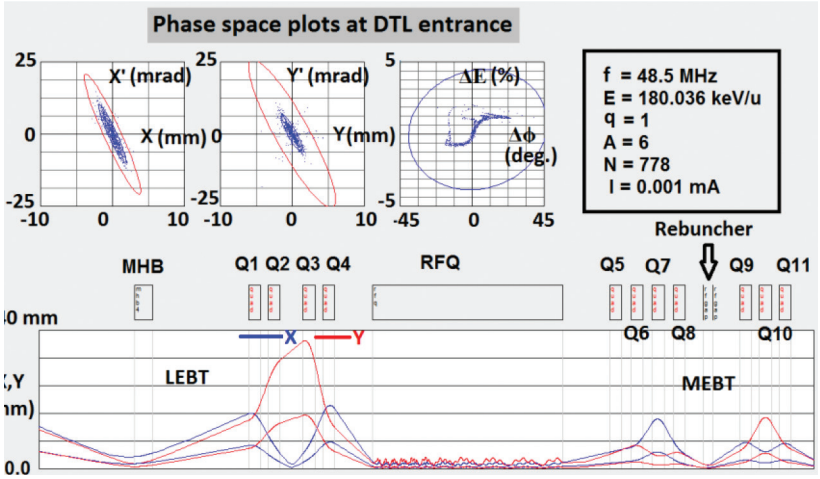


Fig 2.1.22. Beam optics in the combined LEBT and MEBT sections

### 2.1.7.2 Installation of the Low Energy Beam Transport (LEBT) Section upto RFQ

The installation of HCI continued this year and the remaining LEBT components have been installed in the beamline. The point wise summary of the same is given below:

1) **Diagnostic Units:** Two beam diagnostic units have been made consisting of a NEC BPM module and a pair of NEC beam slits assembled onto newly designed vacuum chambers. These diagnostics would be used for pre and post bunched beam diagnosis.

2) **Pumping Chamber:** A new pumping chamber has been designed and fabricated and it is installed with 1000 lps maglev turbo pump. A Danfysik make water cooled insertable Faraday cup is also mounted on DN 100 CF port on chamber top.

3) **Fast Faraday Cup (FFC) chamber:** A vacuum chamber for the installation of Fast Faraday cup has been designed and fabricated. FFC sits on the top DN 150 CF tapped flange and a port on the side is provided for installing a 600 lps turbo pump. A linear motion feedthrough with an aperture ladder is also installed on a DN 40 CF port towards RFQ side. The aperture protects the RFQ vanes during tuning of beam.

4) **Magnetic Steerers:** A pair of magnetic steerers have been designed and fabricated for installation between the quadrupoles, for beam correction.

5) **Quadrupoles:** It consists of four singlet quadrupoles and for the installation and alignment of these quadrupoles a mounting fixture has been designed and fabricated. All the four singlets are mounted on a single base plate with provision for individual alignment of each of them. A vacuum chamber for the quadrupoles was also made with two edge welded bellows at the ends to provide flexibility in installation within the limited space. Two magnetic steerers have also been installed within the available spaces between singlets.

6) **Multi Harmonic Buncher (MHB):** It has been installed with a newly made alignment and mounting fixture. An ion pump (400 lps), with a gate valve, is also mounted on the side port of the buncher chamber. Because of the gate valve the ion pump runs continuously uninterrupted during venting of the chamber. A BPM-Slit diagnostics is also installed at the entry and the exit of MHB.

7) **RFQ** has been perfectly aligned within 0.5 mm of beam axis.

All the components are mounted firmly on a stand made of standard aluminum profiles assembled and erected as per component load positions, available space and ease of installation. All the critical ports, for BPM, slits, aperture etc., in the vacuum chambers are fabricated within an accuracy of 0.5 mm. The components are aligned within 0.5 mm of beam axis. A compact diagnostic box, BPM-Faraday cup assembly, is installed at the exit of RFQ for post acceleration beam diagnostics. We have achieved an ultimate vacuum of 5.0 x $10^{-10}$ torr with two turbo pumps of capacity 1000 lps and 600 lps and an ion pump of 400 lps, installed in the LEBT section.

All beamline components (FFC, Faraday cup, BLV, steerers, quadrupoles, etc.) of this section are controlled by VME based control system. These components have been interfaced with the VME control system and all control and status read signals are available on the remote control console. Digitized BPM signals from the high voltage platform have been provided in the control console through BPM digitizer. All other BPM signals have also been brought in the control console.

### 2.1.8 Instrumentation development

#### 2.1.8.1 Commissioning of HCI Multi-Harmonic Buncher (MHB) RF field Controller

S. K. Suman, V. V. V. Satyanarayana, Rajesh Kumar

(a) (b)

Figure:2.1.23(a) MHB Controller installed in HCI control console (b) the assembled controllers

The in-house developed Low Level RF (LLRF) based 12MHz saw tooth wave generator and controller was put to operation for the first time. At the time of initial powering the MHB was driven in open loop through RF amplifiers to observe the transfer function of the RF amplifiers, the MHB tanks and the pickup loop. This is done because every harmonic being of a different frequency, has different gain in the RF amplifiers and undergoes different phase shifts and losses in tank circuits. This information is used to adjust the gain and operating points of the individual feedback loops of every harmonic and to scale the pick-up signal before feeding it to the controller for closed loop operation. After setting loop gains the controller was set to closed loop operation for auto control of phase and amplitude of the MHB field. The phase and amplitude of the MHB are stable over time and the control flexibility is proved to be very useful in optimizing the bunch width. The controller and the best optimised pickup waveform, which is the derivative of MHB voltage, and the corresponding saw-tooth drive is shown in the figure 2.1.23 (a). Three more controllers have been assembled, one as a spare for the HCI-MHB and two for the Pelletron MHB setup augmentation. The assembled MHB controllers are shown in figure 2.1.23 (b).

### 2.1.8.2 Maintenance of the Vacuum Tube based 48.5 MHz/120 kW RF amplifier

S. Venkataramanan, Rajesh Kumar, C.P. Safvan

After receiving the amplifier from the supplier, it was tested at 75kW with a dummy load in year 2015 to certify the operation and performance. This year the amplifier has been shifted to final location to power the RFQ cavity. All the metering parameters and trip points were recalibrated. During this calibration process, the grid power supply of final power amplifier was repaired for partial failure in the rectifier section. After that the amplifier was operated up to 40kW power. During operation with the RFQ cavity a serious problem was observed that the amplifier started tripping even at very low output power when the line voltage was low. This was the indication of change in the biasing conditions of the amplifier. The low AC line voltage has changed the bias power supplies as all of these are unregulated. The bias power supplies have been readjusted and in particular, the final power amplifier plate voltage has been increased from 11kV to 12.5kV, which enables the amplifier to work over a wide range of line voltage. Presently the Power amplifier is connected to the RFQ cavity and is successfully powering it.

### 2.1.8.3 LLRF control for High Current Injector RF Cavities

S. K. Suman, Rajesh Kumar, C.P.Safvan, R Mehta and BP Ajith Kumar

The first prototypes of the GDR type analogue based LLRF amplitude, phase and frequency controls for the room temperature cavities of HCI project were developed last year. This year all these controls were operated with the RFQ cavity and were used to control the RF field of the cavity. A lot of operational and functional experience was acquired during operation. The control accuracy of amplitude and phase loop meets all the stability requirements. Initially the RFQ cavity was energised in open loop to avoid tripping of the LLRF control because of initial perturbations in the cavity. The RF power was increased in open loop up to the desired level while simultaneously tuning the frequency using the frequency tuner control in close loop. After thermally stabilizing the system, the controller was put to close loop mode for auto control of the phase and amplitude of the cavity field.


Figure:2.1.24 amplitude and phase controllers for the RF cavities.

One serious functional limitation observed was regarding the tripping of the control loop while changing over from open loop operation to close loop operation at desired RF power. The reason of tripping was the large feedback error which was developed in the feedback error amplifier during open loop operation due to its high gain. It was not possible to null the error in open loop before closing the control loop. To operate in close loop the cavity has to be brought back to low power, then close the loop at low power and again increase it to the required power. In this way we were losing the thermal stability acquired while operating in the open loop, although the Controller was operated in close loop by closing the loop at low power. The power was increased slowly, giving enough time after every increase to thermally stabilize the cavity.

Simultaneously the design of the phase and amplitude controller was modified to enable smooth transfer from open lop to close loop at high RF power. The new modification has made the GDR control scheme functionally equal to SEL loop, where the open loop to close loop transfer is easily possible. Additionally the new controller has been provided with the remote control facility, maximum possible controls and monitors are provided for remote operation. Three units of the modified controller has been assembled (figure 2.1.24), one for 97 MHz operation to be used with DTL cavity and two units for 48.5MHz operation to be used with RFQ and Spiral Buncher cavities. The assembly of these controllers is in progress.

### 2.1.9 Compact Diagnostic System for MEBT Section

R. V. Hariwal, S Kedia, R. Mehta

We have developed a Compact Beam Diagnostic System (CBDS) indigenously within 70 mm of longitudinal length. The motivation behind the development of such a compact devices for High Current Injector (HCI) was due to the space constraint in the MEBT section and to preserve the transverse and longitudinal emittances at the entrance of Drift Tube Linac (DTL). CBDS comprises exclusively Faraday cup (FC) and Slit Scanner (SSC) to determine the beam current and beam profile respectively. It has also been planned to develop a Capacitive Pick up (CPU) to measure bunch length. The mechanical and electrical designs of these elements have been verified earlier from CBDS online test with various ion beams. The 3D design of CDB, FC and SSC has been shown in Figure 2.1.25.

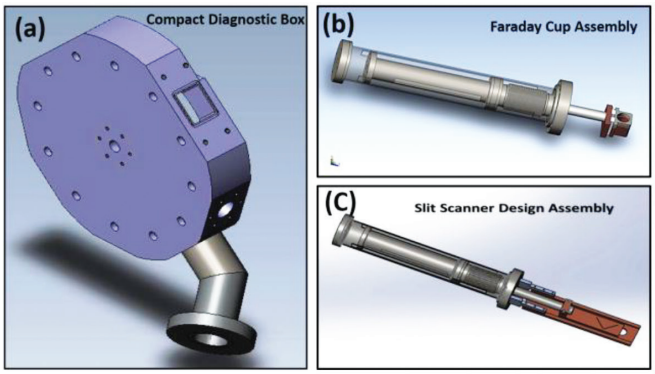


Figure 2.1.25. 3D design of (a) CDB, (b) FC and (c) SSC.

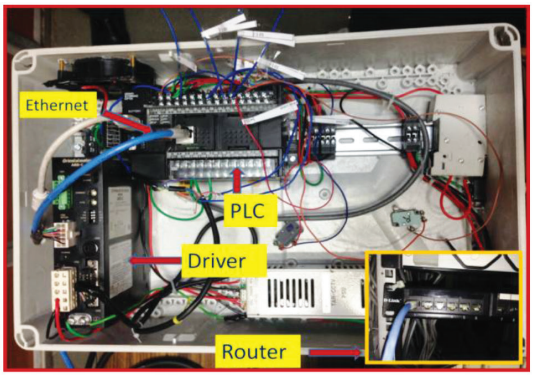


Figure 2.1.26. PLC based stepper motor controller module for CBDS operation.

We have also developed a Programmable Logic Controller (PLC) based electronic module for CBDS operation and control. The program is written in the Python language. The module is able to control the direction, speed, acceleration and number of steps during the online operation. The PLC based electronic module has been shown in Figure 2.1.26. The PLC programming and data processing during the experiments have been performed by using Python/ LabVIEW programs. The linear movement of SSC have been carried out using the stepper motor and their positions were controlled using two limit switches.

CBDS have been previously tested successfully in LEIBF beam line with various ion beams like Ar, N, C and O at different energy and current. The CBDS was later installed in the LEBT section of the HCI beam line and tested with the 30 keV $^{16}O^{2+}$ ion beam. The installed CBDS and ion beam profile are shown in the Figure 2.1.27. The beam profiles have been represented by 2D graph between the beam intensity and corresponding beam positions. The current and beam profile results validated the structural design features of the CBDS for its successful operation.

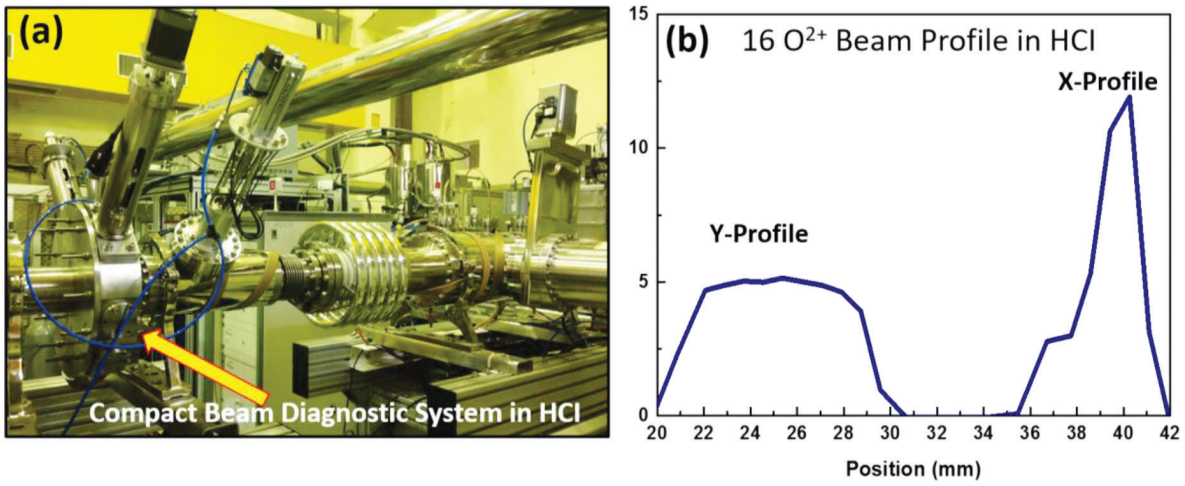


Figure 2.1.27. (a) The installation of CBDS in the HCI and (b) beam profile results for $^{16}O^{2+}$ ion beam.

The Capacitive pickup development was taken up to measure the beam bunch length. We have developed a CPU having design parameters compatible to the energy of HEBT section. CPU has been designed and fabricated having the longitudinal length of ~40 mm. 3D solid work design, fabricated CPU and offline test results have been shown in Figure 2.1.28.

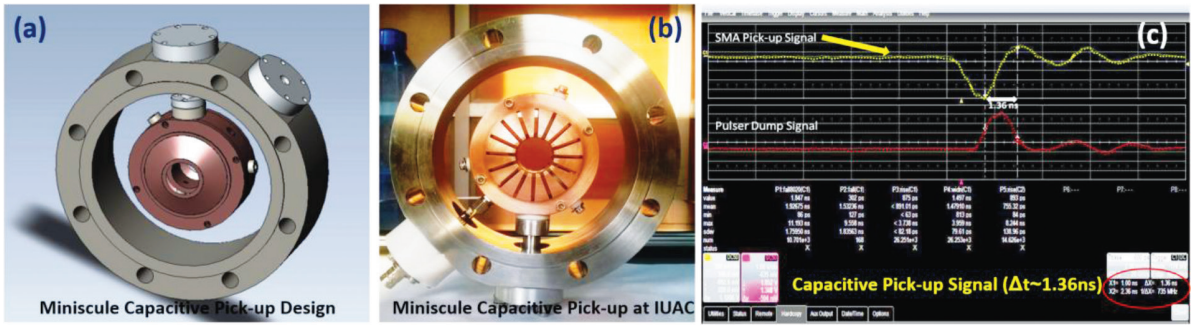


Figure 2.1.28. (a) 3D design of CPU, (b) Prototype CPU and (c) Offline result with ~1 ns bunch length.

CPU has been made of the SS304 material and this can be easily mounted with the 6 " flanges from both sides in the 4'' beam transport line. The inner cylinder is electrically isolated from the outer coaxial cylinder using three insulated ceramics. Further tests on the device are underway.

### 2.1.10 Burn-In Test of 20 KW Solid State RF Amplifier at IUAC

V. V. V. Satyanarayana, Paramananda Singh, Y. Mathur and U. K. Rao

A 20 kW solid state RF amplifier was procured from dB Electronica, Italy. The amplifier was commissioned at IUAC and burn-in test has been successfully completed. The test was carried out for more than 100 hours of continuous run at its maximum rated output power 20 kW. A water-cooled 50 Ohm dummy load was connected to the output of the amplifier. The power output of the amplifier was at the power level of 20.00 kW to 20.05 kW during entire run. Parameters like power sweep for linearity, frequency sweep for bandwidth, phase-plot, and harmonics were measured during the test. Output power of the amplifier was cross-checked with a standard directional coupler from Bird Electronics, USA which was connected at the output port of the amplifier. The stability as well as the capability of the utility systems like electrical and cooling-water systems has also been tested. The following table gives the test details. Figure 2.1.29 shows the setup and figure 2.1.30 shows the harmonic measurement.

**Table**

| Parameter | Value |
|---|---|
| Test Run time | 108 hours Continuous |
| Output Power measured | (20.00 - 20.05) kW |
| Signal generator input | + 0.2 dBm @ 97MHz |
| Bandwidth | 37 MHz (70MHz – 107MHz) |
| Phase plot | $\pm 5^0$ |
| Harmonics | < -46.5 dBc (3rd Harmonic) |
| AC to RF Efficiency | ~62% at 20 kW output power |
| Interlocks tested | Water-flow, emergency stop, auxiliary interlock etc., |
| Water IN/OUT Temperature<br>Pressure<br>Flow | $20^0$C / $23^0$ C<br>3.5 Bar<br>78.4 lpm |
| AC mains | 388V 49A per each phase |

Fig.2.1.29 Burn-in Test at IUAC with 50 Ohm Load

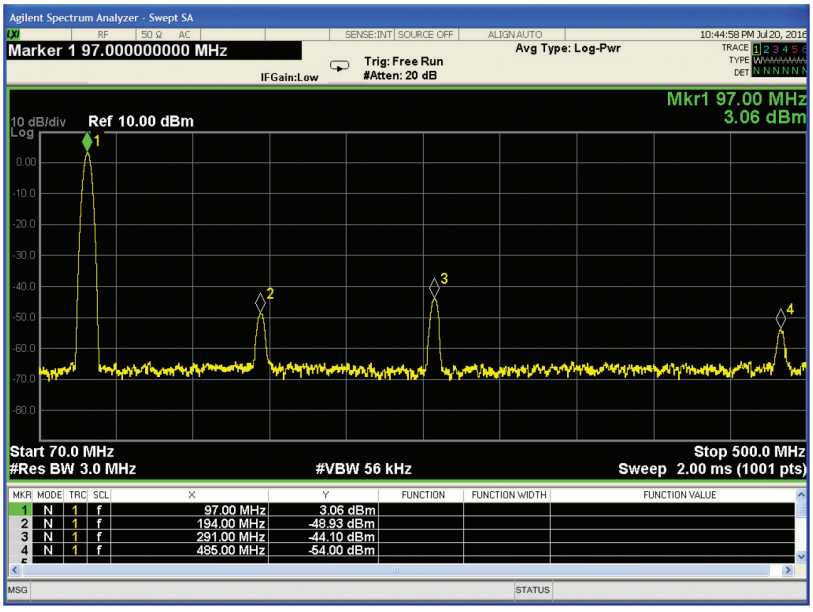


Fig. 2.1.30 Harmonics on Spectrum Analyzer

## 2.2 DEVELOPMENT OF A COMPACT FREE ELECTRON LASER

### 2.2.1 Delhi Light Source based on Free Electron Laser principle

S.Ghosh[1], J.Urakawa[2], N.Terunuma[2], S.Fukuda[2], M.Fukuda[2], A.Aryshev[2], B.K.Sahu[1], P.Patra[1], S.R.Abhilash[1], J.Karmakar[1], B.Karmakar[1], D.Kabiraj[1], N.Kumar[1], A.Sharma[1], V.Joshi[1], G.K.Chaudhari[1], T.Rao[5], V.Naik[4], A.Roy[4], R.K.Bhandari[1] and D.Kanjilal[1]

[1]Inter University Accelerator Centre (IUAC), Aruna Asaf Ali Marg, New Delhi, India
[2]High Energy Accelerator Research Organization, KEK, Tsukuba, Japan
[4]Variable Energy Cyclotron Center, Kolkata, India
[5]Brookhaven National Laboratory,USA

#### 2.2.1.1 Introduction

The demand for intense Terahertz radiation to perform studies in various fundamental and applied research fields is increasing steadily in India. To address the requirement, a compact Free Electron Laser (FEL) named as Delhi Light Source (DLS) [1] is under construction and commissioning at Inter University Accelerator Center. During the first phase of the project, a normal conducting (NC) photocathode electron gun will be used to generate the pre-bunched electron beam of energy ~ 8 MeV which will be injected in to a short undulator magnet to produce THz radiation in the frequency range of ~ 0.15 to 3 THz.

#### 2.2.1.2 Development of various subsystems of Phase-I of DLS

##### 2.2.1.2.1 Beam Transport simulation of Phase-I

The beam transport simulation done initially by ASTRA [2] and finally by General Particle Tracker (GPT) [3] code aims at the generation of the frequency ranging between 0.15 – 3.0 THz. The calculation includes the electron microbunch generation at the RF photo cathode, accelerating the beam through the RF gun, focussing it through the solenoid and quadrupole singlet, transporting it through various beam diagnostic devices acting as drift tube and finally injecting it into a planar permanent magnet Undulator. The beam profile in X and Y direction simulated for both the frequencies of 0.15 and 3.0 THz are shown in figure 2.2.1(a) and 2.2.1(b) respectively. The undulator magnet starts at 2.3 m and ends at 3.8 m from the location of the photocathode.

The output data from GPT has been used to calculate the bunching factor (BF) at the entrance of the undulator magnet shown in figure 2.2.1(c) and the parameters are optimized to make the BF peaks at ~ 0.15 and 3.0 THz. The calculated power generated from 2 and 16 microbunches for 0.15 and 3.0 THz respectively is shown in figure 2.2.1(d) which shows that the length of the undulator need not to be more than of 1.5 metre to extract maximum radiation power out of the electron micro-bunches. An in-house code is being developed to calculate the bunching factor and the power generated from the wiggling electrons inside the undulator magnet. The simulated beam parameters from ASTRA and GPT to generate two extreme radiation frequencies (0.15 and 3 THz) are given in Table-1.

##### 2.2.1.2.2 The Copper cavity as the electron gun

The electron beam is generated from a photocathode placed inside an RF electron gun. The electron beams produced at the photocathode will be immediately accelerated to a maximum energy of ~8 MeV by an accelerating field of ~110 MV/m in RF gun. The design of the copper cavity is similar to those at BNL and KEK [4, 5] and was developed in collaboration with KEK, Japan. The cavity is now under evacuation and will be installed shortly in the beam line of DLS. The details of the cavity and its bead pull data are shown elsewhere [1]. The quality factor and the frequency of the copper cavity had been measured to be ~15,000 and 2859.795 MHz @ 24.5$^0$C respectively. The operating temperature of the copper cavity will be kept at 30$^0$C during operation, so the resonance frequency of the cavity can easily be adjusted to 2860 MHz.

**Table1: Estimated beam parameters for Phase-I of DLS**

| | | |
|---|---|---|
| Two extreme Radiation Frequency (THz) | 0.15 | 3 |
| Electric field – e-gun (MV/m) | 55 | 110 |
| Launching Phase (deg) | 30 | 30 |
| Electron Energy (MeV) | 4.11 | 8.06 |
| Energy Spread (keV) | 70 | 34.5 |
| e-beam FWHM @ Cathode (fs) | 100 | 100 |
| Total Charge (pC)/microbunch | 15 | 15 |
| Number of microbunches | 2 | 16 |
| Separation in ps between Microbunches @ Cathode | 8.7 | 0.424 |
| B-solenoid (T) | 0.120 | 0.231 |
| Quad field (T/m) | 0.071 | 0.120 |
| e-beam FWHM @ | | |
| Undulator Entrance (fs) | 350 | 117.5 |
| Peak Current (A) at PC | 150 | 150 |
| Beam Area (mm2) | 3.2 | 4 |
| Norm. beam emitt.- x (mm-mrad) | 1.051 | 1.164 |
| Norm. beam emitt.- y (mm-mrad) | 12.89 | 1.404 |

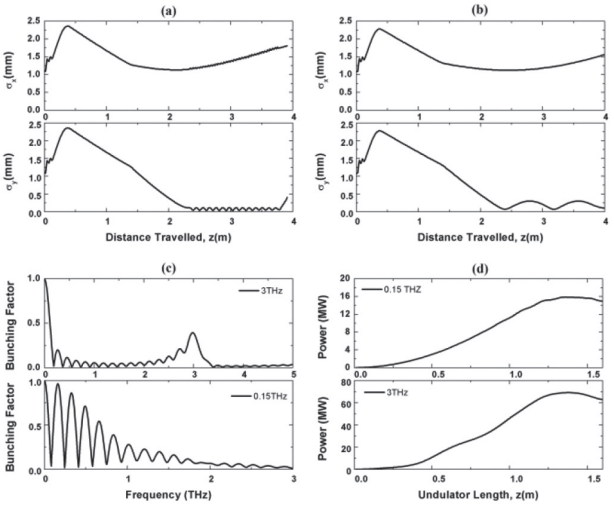


Figure 2.2.1: (a), (b) Variation of beam profile, σx,σy upto the end of the undulator for 0.15 and 3 THz (c) Bunching factor at the entrance of undulator for 0.15 & 3 THZ (d) THz power at the end of the undulator for 0.15 & 3 THz

### 2.2.1.2.3 The Photocathode deposition system

The electron beam from the RF gun will be produced initially from the copper photocathode. Later on, to increase the electron current and hence the power of radiation, semiconductor photocathode will be used at IUAC. For that, the development of the complete deposition system to produce the semiconductor photocathode has been initiated and the assembly drawing of the deposition system is prepared (figure 2.2.2). In the case of deposition of semiconductor (e.g. $Cs_2Te$) thin film on a metal substrate (e.g. Mo), first the photocathode plug will be loaded in chamber#1 and the active surface of the plug will be thoroughly cleaned with the high power laser. Then it will be transported to chamber#2 for deposition of Te (~ 10 nm thickness) followed by Cs (~ 90 nm) subjected to the maximisation of the measured Quantum Efficiency (QE). The deposited photocathode will be shifted to the storage chamber (chamber#3) which can store up to six photocathode. Finally the individual photocathode will be brought in to the insertion chamber#4 and prior to its insertion in to the RF cavity, its surface is to be evaluated by another measurement of QE in the chamber#4.

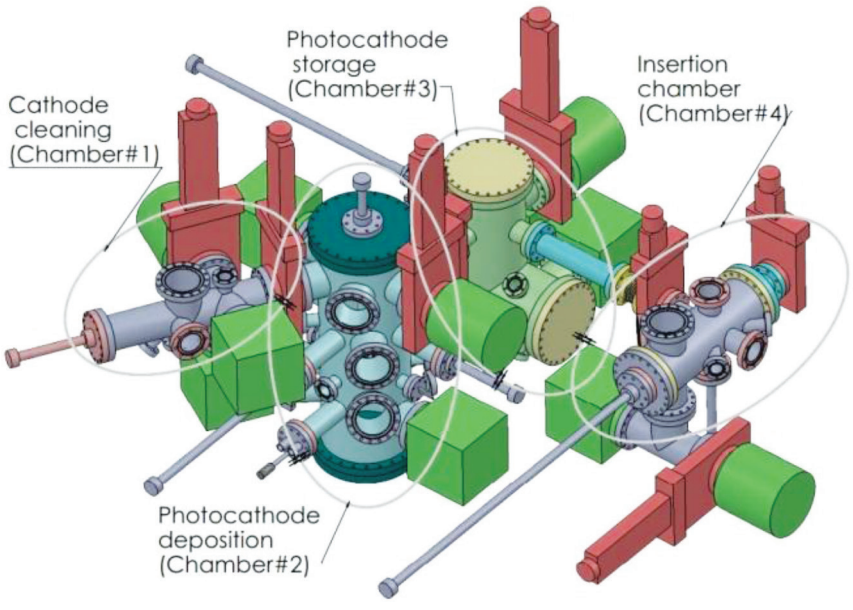


Fig 2.2.2 Schematic of Photocathode deposition System

### 2.2.1.2.4 RF Gun Laser system

High power pulse laser beam is necessary to illuminate the photocathode to generate the electrons. With the recent progress in fiber laser systems, it is decided to develop a fiber laser system for DLS. The specification of an appropriate fiber laser system suitable for our application is currently being finalised. As per the design criteria, each laser pulse will be split in to 2, 4, 8, 16 micro-pulses to generate 'comb beam' with the separation of a few hundreds of femtosecond. There will be a provision to precisely vary the separation between successive microbunches to enhance the intensity of the THz radiation.

**Table - 2. The laser parameter chosen for the Phase-I of DLS**

| System | Energy/ pulse (UV) | Cathode | No of Microbunches | Available charge/ pulse (pC) | Microbunches & reqd. charge/ per microbunch | Pulse width (fs) |
|---|---|---|---|---|---|---|
| Fiber Laser assembled @ KEK | 0.9, 0.4, 0.19, 0.1 uJ | Cu | 2, 4, 8 & 16 | 1.8, 0.8,0.38, 0.2 | 16 no, 15 pC | ~200 |
| | | Cs2Te | 2, 4, 8 & 16 | 900, 400, 190, 100 | 16 no, 15 pC | |

### 2.2.1.2.5 RF system for the electron gun (Copper cavity)

The RF system of DLS is governed by the beam stability requirement of the system that includes mainly the RF phase stability of 0.1 degree and amplitude stability better than 0.01%.The RF system consists of a Low Level RF (LLRF) section and high power RF system containing Klystron and Modulator to power the RF cavity. The high power RF pulse should have the pulse flatness to match the beam stability requirement. There will be additional control to make the clock of the laser oscillator synchronized with the LLRF system. The high power RF system including the klystron, solid state modulator, circulator, waveguide, etc. are ordered and then it will be delivered around March 2018. The design and development of LLRF is being carried out at IUAC in collaboration with BARC, Mumbai.

### 2.2.1.2.6 The Undulator Magnet

The preliminary calculation related to undulator magnet has been initiated and the design of the magnet with the code Radia has been started. As per the design goal, the frequency range of the THz radiation to be produced from Phase-I of DLS is to be confined between 0.15 to 3 THz. If the energy of the electron beam is varied between 4-8 MeV, then for the expected frequency range mentioned above, the tentative parameters for the undulator has been calculated and is given in Table-3. The fabrication of the magnet will be started shortly and it is intended to develop the same in collaboration with a well reputed company which is specialized in undulator magnet.

**Table-3 The main parameters of the undulator magnet to produce THz radiation**

| $\lambda_R$ (~mm) | Freq. to be Produced (THz) | Electron Energy (MeV) | $\lambda_U$ (mm) | K – value | $B_u$ (T) | Required gap (mm) |
|---|---|---|---|---|---|---|
| 2.0 | 0.18 | 4 | 50 | 2.90 | 0.620 | 20 |
| 0.1 | 3 | 8.25 | 50 | 0.59 | 0.126 | 46 |

### 2.2.1.2.7 Beam line design of Phase-I

The initial design of the beam line is shown in figure 2.2.3. The beam optics calculation shows that a solenoid magnet placed after the electron gun will focus the electron beam uniformly at the undulator magnet. In addition,

a singlet quadrupole magnet is necessary to focus the beam in the vertical direction as the height of the beam pipe inside the undulator is limited to < 20 mm (including the wall thickness). Beam optics and beam diagnostic devices have been finalized and they will be installed at the appropriate places of the beam line of DLS as shown in figure 2.2.3.

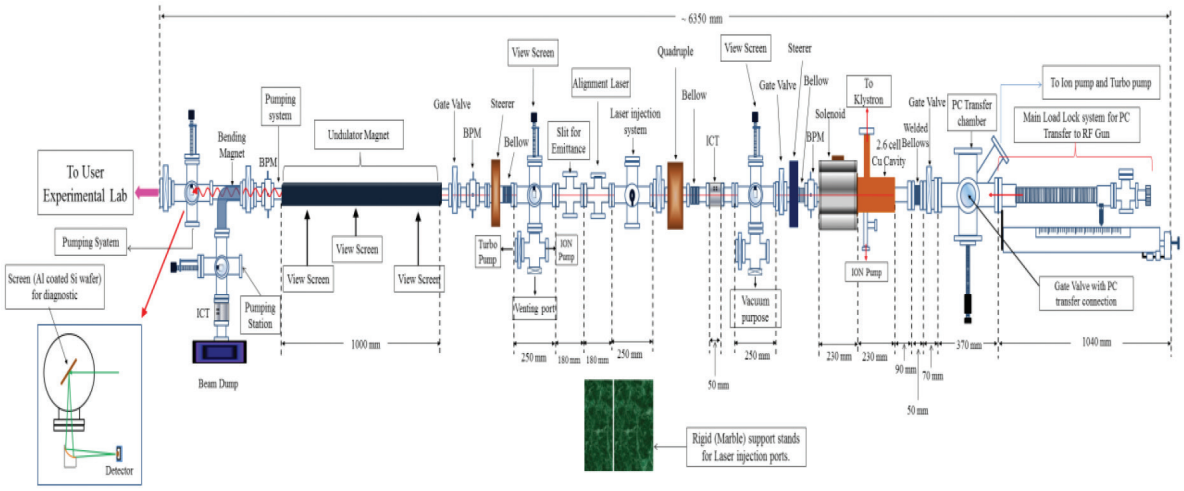


Figure 2.2.3. The proposed beam line design to produce THz from the first phase of DLS

### 2.2.1.2.8 Design of Solenoid magnet for Delhi Light Source

Sarvesh Kumar, G. Rodrigues, S. Ghosh, A. Mandal

A solenoid magnet has been designed to focus 8 MeV electron beam to the middle section of the undulator magnet (K < 1). The magnet is water cooled. The specifications of the magnet are shown in Table 1. Order for the magnet along with power supply has been placed with Danfysik, Denmark.

**Table-1 Specifications of Solenoid Magnet**

| Parameters | Specified Values | Simulation Values |
|---|---|---|
| Maximum magnetic field at the solenoid's centre | 0.35 T | 0.35 T |
| Physical length | ≤ 240 mm | 234 mm |
| Overall diameter | ≤ 480 mm | 307.3 mm |
| Effective length | ~ 200 mm ± 2% | 200 mm |
| Bore diameter | 76 mm, It should fit over 2.75" flange | 76 mm |
| Axial field at a distance of 200mm from the solenoid's centre | < 30 Gauss | 24 Gauss |
| Field homogeneity | ~ 5 x $10^{-3}$ within ± 20 mm around the middle of the solenoid along the transverse and longitudinal direction | <0.1% longitudinally and 0.3 % radially |

### 2.2.1.3 Present status of the Phase-I of Delhi Light Source

The entire accelerator and experimental facility is going to be installed in a recently built class 10000 clean room. The copper cavity has been fabricated and tested and is ready to be installed in the beam line. The design of the photocathode deposition chamber and the photocathode in-vacuum transfer mechanism inside the cavity has been finalized and an expression of interest has been invited from the appropriate companies interested to manufacture the device. The specifications for Klystron and Modulator to power the copper cavity were finalized, tender was floated and the purchase order was placed. The complete device will be delivered at IUAC at the beginning of 2018. The design of the RF and control system at the block diagram level is going on. The high power fiber laser system is being developed in collaboration with KEK, Japan. The design and procurement of Undulator and other electromagnets has been started. The beam transport calculation has been done with

ASTRA and currently being fine-tuned with GPT code to configure the beam line components. The complete facility to provide electron beam (~ 8 MeV) and THz radiation is expected to be operational by end of 2018 and 2019 respectively.

**REFERENCES**

[1] S. Ghosh et al., Nucl. Instr. and Meth. B (2017) page-358-363
[2] K. Flöttmann, ASTRA, www.desy.de/~mpyflo
[3] General Particle Tracker, http://www.pulsar.nl/gpt/index.html
[4] X. J. Wang et al., Nucl. Instrum. Meth. A356, 1995, p. 159.
[5] A. Deshpande et al., Phy. Rev. Special Topic Accel. Beams, 14, 2011, 063501.

## 2.3 ECR AND MICROWAVE ION SOURCE DEVELOPMENTS

G. Rodrigues,Y. Mathur, Narender Kumar, Kedar Mal, Sarvesh Kumar, P.Kumar, R. Ahuja, U. K. Rao & D. Kanjilal

### A (1) 2.45 GHz microwave ion source developments

A 2.45 GHz Microwave ion source based high flux system was designed, developed and commissioned at IUAC in the year 2015. The facility (figure 2.3.1) was developed to deliver high intensity beam in the energy range of a few hundreds of eV to a few tens of keV. The facility was tested and was able to deliver proton beam with beam current intensity of 210 μA/cm$^2$ at the experimental chamber. The facility was characterized by performing ion implantation experiments followed by Rutherford back scattering experiment on implanted samples along with x-ray measurements for determining the electron energy distribution of the plasma generated inside the plasma chamber. Towards the end of 2015, the facility was down because of the electronics related issues of magnetron power supply. A new magnetron based microwave generator was purchased and tested during the year 2016-2017. A relatively new control system is installed to control the microwave generator while delivering microwaves to the plasma chamber. The facility is again functional and users can perform experiments related to ion beams and plasma characterization.

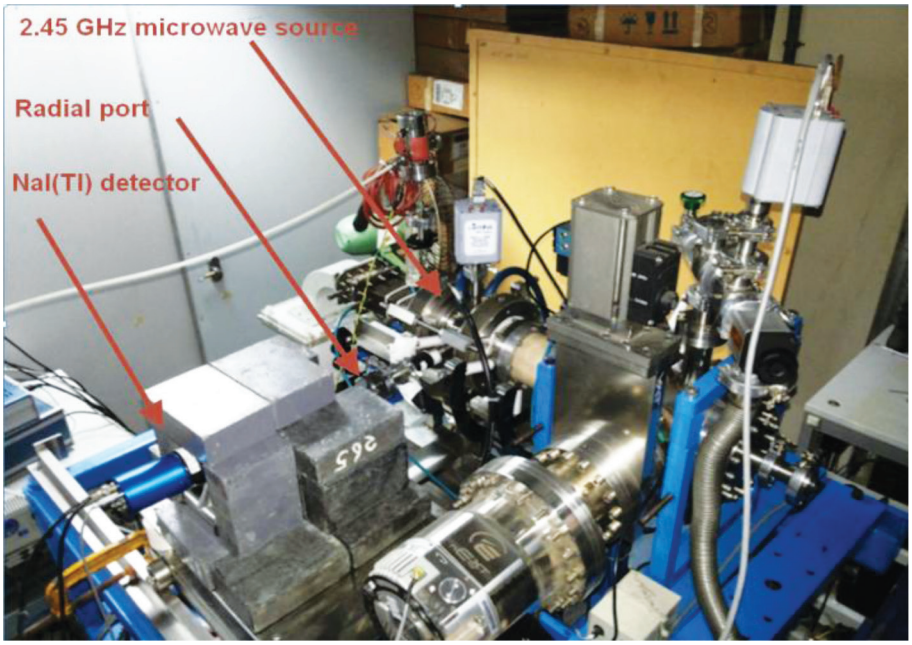


Figure 2.3.1. View of the compact 2.45 GHz microwave ion source based, low energy, high flux facility

In order to make the complete facility as compact as possible, it was felt to incorporate a Wien filter instead of mass analyzing magnet. In year 2016-17, a compact velocity analyzer (Wien filter) was planned to be developed for performing mass separation up to mass 200 a.m.u. The beam optics simulation and mechanical design has been started and some of the preliminary results and calculations are shown in figure 2.3.2. In figure 2.3.2, top figure is the cross sectional view of the Wien filter along with the electric and magnetic field distributions obtained from CST Particle Studio simulations. The Wien filter is planned to incorporate permanent magnets for

the magnetic field. The magnets will have a pole tip field of ~ 1 T with dimensions 100 mm x 40 mm x 10 mm separated by a gap of 70 mm. The voltage requirements were found to be +/- 220 V to +/- 3280 V for masses 200 a.m.u & 1 a.m.u. respectively having energy of 10 keV. Figure 2.3.2 depicts the beam trajectories for four different ion beams having energy of 10 keV energy through the Wien filter. Tuning of both the fields to match them as close as possible using additional electrodes will be an added option in the final design stage.

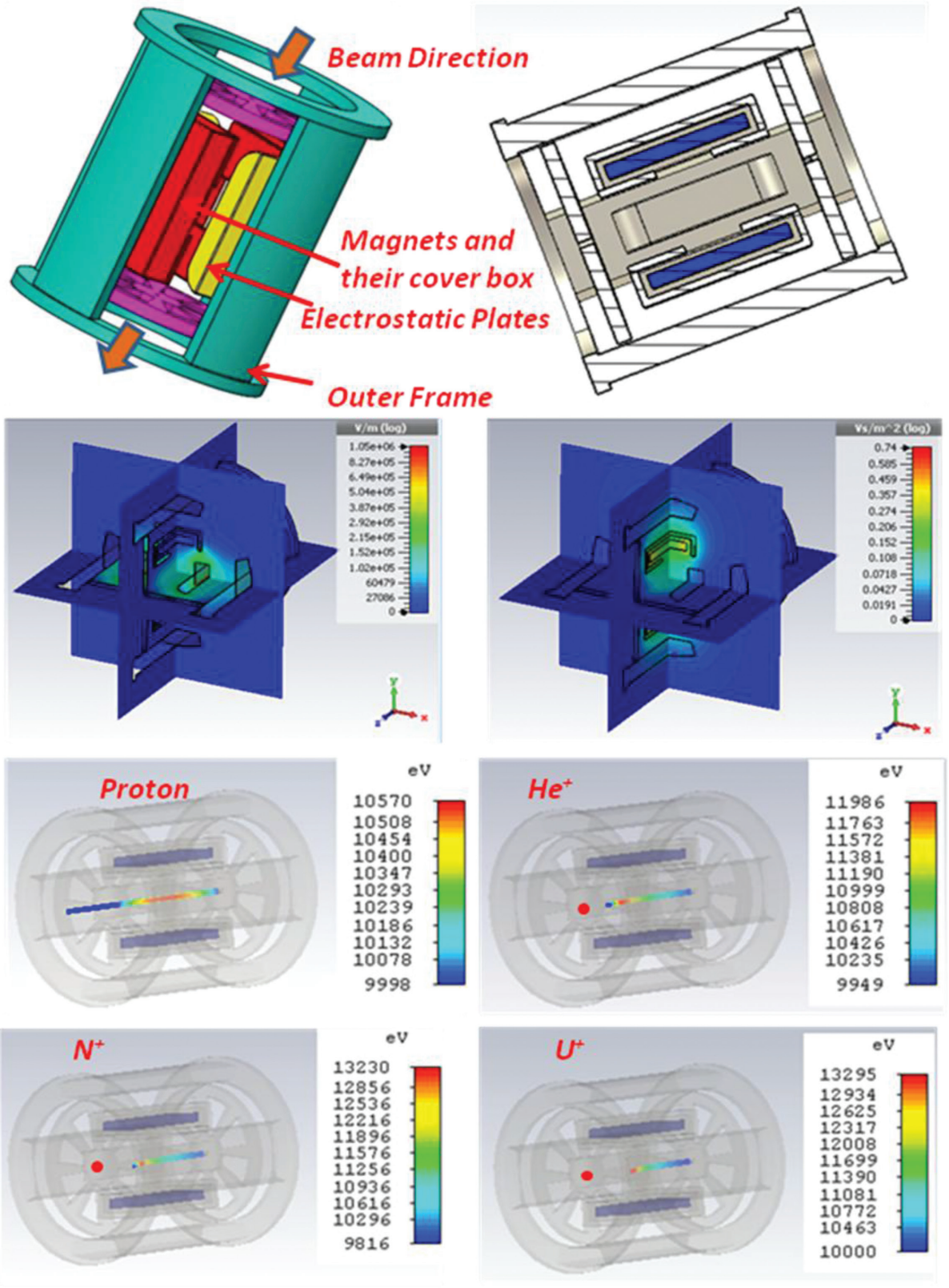


Figure 2.3.2. (Top) 3d mechanical design and cross-sectional view of Wien filter for 2.45 GHz microwave ion source facility along with CST simulations for the system showing the field distributions ; (below) beam trajectory for four ion beams having energy of 10 keV (red dot indicates the position of beam collimator). The electric field is set to deflect all other beams except proton.

## A(2) Electronics and related developments

1) Tested the newly purchased 1kW, 2.45GHz magnetron microwave generator stem using CANBUS software on water cooled dummy load.

2) A controller was developed to operate and monitor 2.45GHz microwave power generators both locally and remotely. It can be operated remotely using this indigenously developed controller via CANBUS, PLC and MODBUS modules.

Figure 2.3.3. Testing of 1 kW microwave generator using indeginously developed controller

## B. Frequency tuning experiments in the 10 GHz NANOGAN ECR ion source

It should be remarked, that after frequency tuning experimental studies were started in the low energy facility using the 10 GHz NANOGAN ECR ion source, we have constantly tried to tune the ion source at alternate frequencies apart from the main operating frequency of 10 GHz. The simple reason was that the gain in the beam intensities has been really substantial as compared to its operation at 10 GHz. Therefore, for various kinds of experiments being carried out at the facility, frequency tuning technique has been adopted in the recent past.

We studied Argon ECR plasma with and without gas mixing at different RF frequencies with optimized source parameters and acquired data for the feasibility of new experiment. These frequencies are 8.59, 8.68, 9.68 and 10.00 GHz. A typical charge state distribution (CSD) of argon plasma mixed with helium at frequency 8.59 GHz is shown in Figure 2.3.4. The highest intensity of $Ar^{8+}$ was 9 euA with only 9W power.

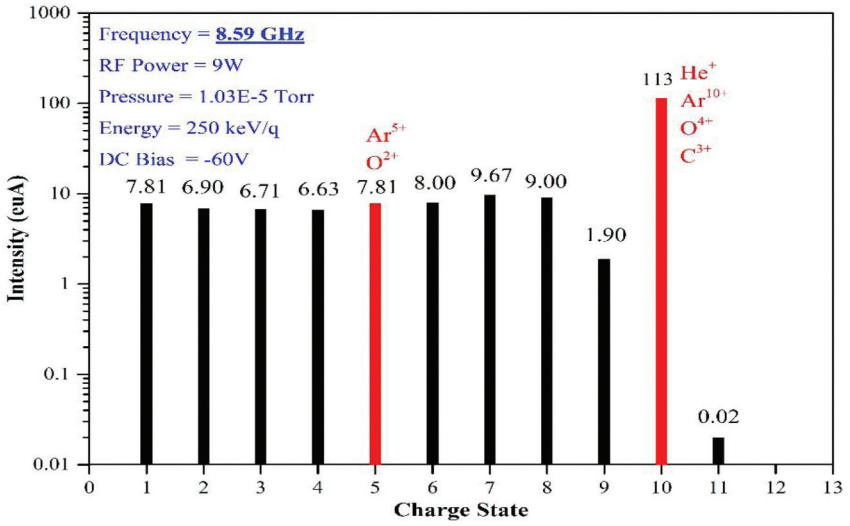


Figure 2.3.4. A typical charge state distribution of argon showing the influence of the helium mixing on the higher charge states at a tuned frequency of 8.59 GHz

3D simulations studies to understand the effects of the plasma permittivity on the frequency will help to correlate the measured beam distributions at various frequencies. This will involve a detailed map of the plasma properties everywhere inside the cavity due to the asymmetry in the field. Since the cavity is operated at a lower frequency range of 9 to 11 GHz, the total number of EM modes is limited without modes being present on the axis. Therefore, hollow beam formation is not possible, unlike those observed in higher frequency ion sources, which have larger diameter cavities. A simulation showing a typical vacuum mode using CST solver is shown on the left hand side of figure 2.3.5. For example, it can be seen that the beam shapes were digitized at selected frequencies when the intensities of argon beams were found high compared to the nearby frequencies. The digitized beam profiles at the beam profile monitor, BPM -1 (before analyzing magnet) are shown on the right hand side of figure 2.3.5.

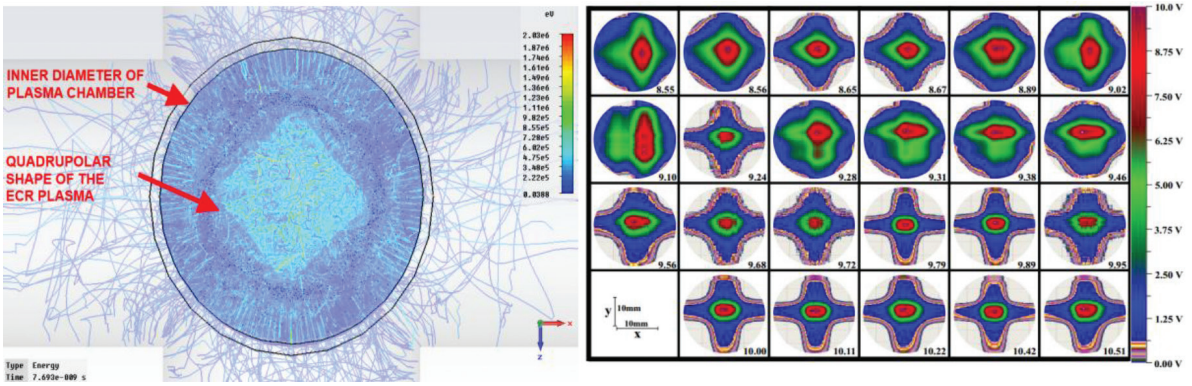


Figure 2.3.5.(Left) Typical simulated vacuum mode of the cavity; (Right) Effect of the various tuned frequencies on the evolving beam shapes measured at BPM-1 (before analyzing magnet).

## C. Gas mixing studies in the NANOGAN ECR ion source

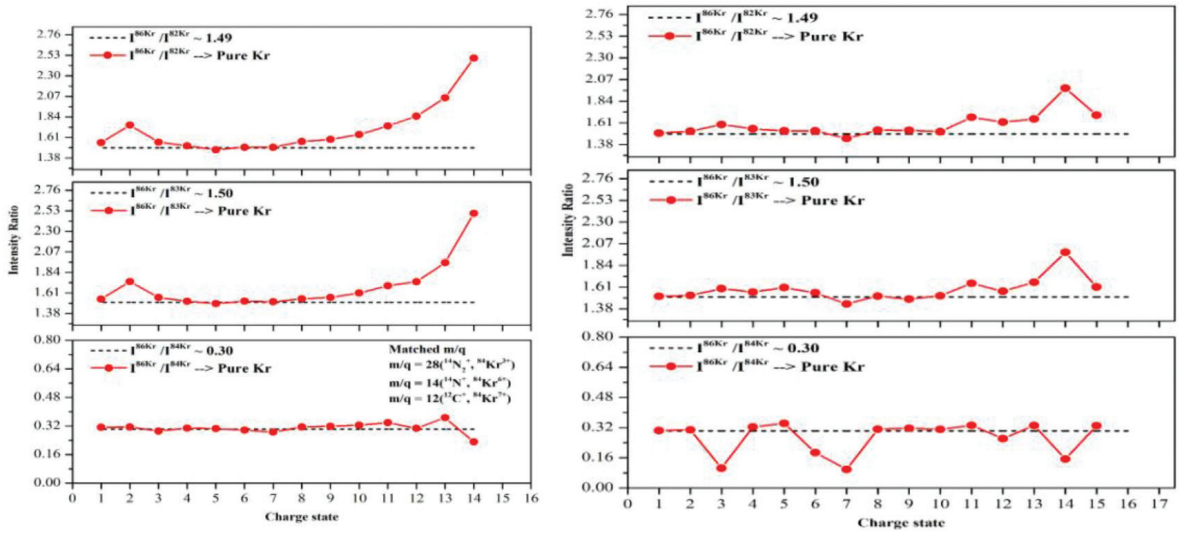


Figure 2.3.6. (Left) Intensity Ratio for pure Kr plasma; (Right) Intensity Ratio for Kr (50%) + $O_2$ (50%) plasma

We studied the charge state distributions of the pure, 25% and 50% oxygen mixed krypton plasma to shed more light on the understanding of the gas mixing and the isotope anomaly. The data were taken in two parts viz. with and without gas mixing. For this experiment, natural krypton gas was used which contains 6 stable isotopes viz. 78, 80, 82, 83, 84, and 86. The source was optimized with pure Kr isotopic plasma for high charge states with high intensity and then full spectrum of pure Kr plasma was recorded. By plotting the intensity ratio of heavier to lighter isotope as a function of charge state, we found that the intensity ratio was increasing with the charge state as shown on the left hand side of figure 2.3.6. This is the so called "anomalous effect" discovered earlier by A.G. Drentje [4]. In second step of this experiment, oxygen gas was introduced into pure Kr plasma by keeping source parameter constant except pressure of both gases. Two sets of data were recorded with gas mixing viz. Kr (75%) + $O_2$ (25%) and Kr (50%) + $O_2$ (50%) plasma. We found that the CSD of Kr isotopes with gas mixing were shifted towards higher charge states in comparison to the CSD with pure Kr plasma. Further, in case of gas mixing, the anomalous effect was disappearing with increased amount of mixed gas as shown in the right hand side of figure 2.3.6. Further experiments are underway to study the influence of an external frequency.

**REFERENCES**

[1] Narender Kumar, G. Rodrigues, Y. Mathur, S. Ohja, R. Ahuja and D. Kanjilal, "Development and test of 2.45 GHz microwave ion source based intense ion beam experimental facility", Vacuum 124, 55-59 (2016).
[2] Narender Kumar, "High Flux 2.45 GHz microwave ion source", ID-386 (T-03), InPAC 2015, BARC, Mumbai.
[3] G. Rodrigues, N. Kumar, Y. Mathur, U. K. Rao and D. Kanjilal, "Alternative way of heating plasmas to increase the densities beyond their cut-off", ID-201, InPAC 2015, BARC, Mumbai.
[4] A.G.Drentje, Rev.Sci.Instrum.,63 (1992)2875